THE JOURNAL OF BIOLOGICAL CHEMISTRY
Vol. 279, No. 5, Issue of January 30, pp. 3620–3626, 2004

Printed in U.S.A.

Structural Role of PufX in the Dimerization of the Photosynthetic Core Complex of *Rhodobacter sphaeroides**

Received for publication, September 10, 2003, and in revised form, October 23, 2003
Published, JBC Papers in Press, October 27, 2003, DOI 10.1074/jbc.M310050200

Simon Scheuring‡, Francesco Francia§¶, Johan Busselez‡, Bruno Andrea Melandri§¶, Jean-Louis Rigaud‡, and Daniel Lévy‡‖

From the ‡Institut Curie, UMR-CNRS 168 and LRC-CEA 34V, 11 Rue Pierre et Marie Curie, 75231 Paris Cedex 05, France and §University of Bologna, Department of Biology, Laboratory of Biochemistry and Biophysics, Via Irnerio 42, Bologna 40126, Italy

Monomeric and dimeric PufX-containing core complexes have been purified from membranes of wild-type *Rhodobacter sphaeroides*. Reconstitution of both samples by detergent removal in the presence of lipids leads to the formation of two-dimensional crystals constituted of dimeric core complexes. Two-dimensional crystals were further analyzed by cryoelectron microscopy and atomic force microscopy. A projection map at 26-Å resolution reveals that core complexes assemble in an "S"-shaped dimeric complex. Each core complex is composed of one reaction center, 12 light-harvesting 1 α/β-heterodimers, and one PufX protein. The light-harvesting 1 assemblies are open with a gap of density of ~30-Å width and surround oriented reaction centers. A maximum density is found at the dimer junction. Based on the projection map, a model is proposed, in which the two PufX proteins are located at the dimer junction, consistent with the finding of dimerization of monomeric core complexes upon reconstitution. This localization of PufX in the core complex implies that PufX is the structural key for the dimer complex formation rather than a channel-forming protein for the exchange of ubiquinone/ubiquinol between the reaction center and the cytochrome *bc1* complex.

In purple photosynthetic bacteria, highly organized transmembrane pigment-protein complexes perform absorption of light and its conversion into chemical energy. Two light-harvesting complexes (LH),[1] LH2 and LH1, ensure the collection of light. Then the excitation energy is funneled toward the special pair of bacteriochlorophylls in the reaction center (RC), followed by an electron transfer from the special pair of bacteriochlorophylls to the ubiquinone (Q) acceptors Q_A and Q_B. After two photoreactions and proton captures, ubiquinol (QH_2) is formed at the Q_B site that dissociates from the RC into the membrane. The bc_1 complex utilizes QH_2 and oxidized cytochrome c_2 as reductant and oxidant, respectively. The net result is a cyclic electron transfer that promotes the formation of a proton gradient across the membrane, which is utilized for ATP synthesis by F_1F_0-ATP synthase (for a review, see Ref. 1).

The mechanisms of excitonic energy migration and photoinduced electron transfer have been studied in detail using biophysical approaches and analyzed at the molecular level following the resolution of the atomic structures of the RC (2), LH2 (3, 4), and the bc_1 complex (5). However, despite the wealth of information available on the individual proteins, their supramolecular organization in the membrane remains undetermined. A crucial issue is the spatial organization between LH1 and RC, forming the so-called core complex, in which the transformation of light energy into charge separation occurs. So far, no atomic model of the core complex is available. Early studies by various electron microscopy (EM) techniques of native membranes of *Rhodopseudomonas viridis* and *Ectothiorhodospira halochloris* have shown a single RC surrounded by a closed circle of light-harvesting molecules (6–8). Organization of LH1 complexes in a closed ring of 16 subunits large enough to house a RC was observed on a cryo-EM projection map of LH1 purified from *Rhodospirillum rubrum* (9). Later, two-dimensional crystals were grown from purified entire core complexes of *R. rubrum* (10–12), *pufX*-deleted *Rhodobacter sphaeroides* (13), and *R. viridis* (14) and analyzed by cryo-EM or negative stain EM, all consistent with a closed LH1 ring of 16 subunits around the RC. More recently, a high resolution atomic force microscopy (AFM) analysis of single molecules in native membranes of *R. viridis* showed LH1 to form a closed ellipse of 16 subunits around a specifically oriented RC (15).

A closed assembly of LH1 raises the question of QH_2/Q exchange between the RC and the bc_1 complex (16). At this point, a protein encoded by the *pufX* gene found in *Rhodobacter* sp. (*sphaeroides* and *capsulatus*) has been shown to be necessary for photosynthetic growth (17, 18) and more specifically to facilitate the transport of reducing equivalent from the Q_B site of the RC to the bc_1 complex (17, 19). In *R. sphaeroides*, this additional peptide PufX is a small protein of 82 amino acids with one membrane span (20–22). Much data led to the hypothesis that the PufX protein is located in the inner α ring of LH1 (20–22), forming a specific channel and/or interrupting the LH1 continuity and thus allowing a facilitated diffusion of QH_2/Q between RC and bc_1 complex. Furthermore, biochemical studies have shown that PufX-containing core complexes could be isolated from *R. sphaeroides* membranes as dimeric structures with a 1:1 PufX/RC stoichiometry and a decreased number of LH1-associated Bchls per RC (23).

The only structural information available about a PufX-containing core complex has been derived from a low resolution

* This study was supported by the Institut Curie, the Commissariat à l'Energie Atomique (Saclay, France), the CNRS, European Economic Community Grant HPRN-CT-2002-00269, and the Ministerio dell'Intruzione, Universita e Ricerca (to F. F. and B. A. M.). The costs of publication of this article were defrayed in part by the payment of page charges. This article must therefore be hereby marked "*advertisement*" in accordance with 18 U.S.C. Section 1734 solely to indicate this fact.

¶ Supported by the Ministerio dell'Intruzione, Universita e Ricerca of Italy Grants PRIN/2001 and FIRB/2001.

‖ To whom correspondence should be addressed. E-mail: daniel.levy@curie.fr.

[1] The abbreviations used are: LH, light-harvesting complex; AFM, atomic force microscopy; Bchl, bacteriochlorophyl; DOTM, 1-*S*-dodecyl-β-D-thiomaltoside; EM, electron microscopy; OG, *n*-octyl β-D-glucopyranoside; Q, ubiquinone; QH_2, ubiquinol; RC, reaction center.

negative stain EM analysis of native two-dimensional crystals of a LH2-deleted *R. sphaeroides* strain (24). This projection map revealed two C-shaped incomplete antenna rings each surrounding one RC. Finally, polarized spectroscopy of *R. sphaeroides* membranes containing or lacking PufX provided evidence that PufX induced a specific orientation of the RC in the LH1 ring as well as the formation of a long range order of LH1-RC core complexes (16, 25). Taking together all of these considerations, PufX is thought to play a key role in the core complex. One challenge now being addressed is the localization of PufX in the core complex to get a deeper insight into its implication in the structure-function relationship critical for bacterial photosynthesis.

In order to understand the role of PufX in the core complex, we have performed a structural study by two-dimensional crystallization of monomeric and dimeric PufX-containing core complexes isolated from wild-type *R. sphaeroides*. The purified complexes were analyzed by sedimentation and absorption spectroscopy. Two-dimensional crystals were produced by detergent removal from protein/lipid/detergent mixtures and analyzed by cryo-EM and AFM. Both monomeric and dimeric core complexes reassemble in dimeric PufX-LH1-RC complexes when reconstituted in lipid membranes. The cryo-EM projection map, revealing protein densities of trans-membrane segments, showed an "S"-shaped core complex dimer. The LH1 assemblies are open with a lack of protein density within the gaps, the dimer junction has a stronger density than the rest of the "S", and the RC reveals an asymmetric density maximum within the open LH1. Taking all information together, we propose a model in which PufX is located at the dimer junction and directly involved in the formation of the supramolecular assembly of core complexes rather than providing a direct pathway for the QH_2/Q exchange.

EXPERIMENTAL PROCEDURES

Materials—All phospholipids and detergents were of highest purity and were purchased from Avanti Polar Lipids and from Fluka or Anatrace, respectively. Bio-Beads SM2 (25–50 mesh) from Bio-Rad were extensively washed with methanol and water before use as described (26). All other reagents were of analytical grade.

Isolation and Purification of the Monomeric and Dimeric Complex—Core complexes from semiaerobically grown *R. sphaeroides* strains with and without PufX were isolated as described previously (23), except that after the washing step in 2 M NaBr, 0.2 M sucrose, membranes were directly resuspended at 10 mg/ml protein and extracted with 3% *n*-octyl β-D-glucopyranoside (OG) and 0.5% sodium cholate. After extraction, the supernatant was run on a sucrose gradient (10–40%) in buffer glycyl-glycine (50 mM), pH 7.8, 0.6% OG, and 0.2% sodium cholate. As previously shown (22, 23), three major bands were isolated, including an LH2-containing band and two PufX-containing bands corresponding to the monomeric or dimeric core complexes.

For detergent exchange, before two-dimensional crystallization, the monomeric or dimeric core complexes purified on an OG/cholate sucrose gradient, were dialyzed against a buffer containing 50 mM glycyl-glycine, pH 7.8, 0.1% 1-*S*-dodecyl-β-D-thiomaltoside (DOTM). The polypeptide composition of the final fraction was controlled by SDS-polyacrylamide gel electrophoresis and Coomassie staining (27).

Reconstitution and Two-dimensional Crystallization—Purified LH1-RC-PufX complexes at 0.4 mg/ml in a buffer containing 0.1% DOTM, 200 mM NaCl, 50 mM gly-gly, pH 7.8, were mixed with egg phosphatidylcholine/egg phosphatidic acid (9:1, mol/mol) at lipid/protein ratios between 0.75 and 1 (w/w). The lipid/protein/detergent mixture was allowed to equilibrate overnight in the dark. Detergent removal was performed through two successive additions of 5 mg of SM2 Bio-Beads/50-μl sample, for 12 h each, at 4 °C (28). Crystals were then withdrawn and kept at 4 °C for EM and AFM analysis.

Electron Microscopy—Negative stain and cryo-EM were performed using Philipps CM120 and Philipps FEG200 electron microscopes operated at 120 and 200 kV, respectively. Two-dimensional crystals were adsorbed for 1 min on glow-discharged carbon-coated 300-mesh grids. Two-dimensional crystals were either negatively stained with 1% uranyl acetate, or quick frozen in liquid ethane for cryo-EM analysis. The latter were transferred into the electron microscope using a Gatan cryo transfer system. Images were directly assessed using low electron dose procedures at a magnification of ×40,000 on a 14-μm 2048 × 2048-pixel Gatan slow scan CCD camera corresponding to 3.5 Å/pixel.

Atomic Force Microscopy—Mica prepared as described (29) was used as support and freshly cleaved before every experiment using Scotch tape. 3 μl of two-dimensional crystal solution (0.1 mg/ml) was injected into the adsorption buffer drop (10 mM Tris-HCl, pH 7.6, 200 mM KCl, 5 mM $MgCl_2$) on the mica surface. After 2 h, the sample was carefully rinsed with recording buffer (10 mM Tris-HCl, pH 7.6, 200 mM KCl). Imaging was performed with a commercial Nanoscope III AFM (from Digital Instruments, Santa Barbara, CA) equipped with a 150-μm scanner (J-scanner) and oxide-sharpened Si_3N_4 cantilevers with a length of 100 μm (k = 0.09 N/m; Olympus Ltd., Tokyo, Japan). The AFM was operated in contact mode applying forces of <0.2 nN at scan frequencies around 3 Hz.

Image Processing—Cryo-EM images of two-dimensional crystals recorded on the CCD camera were treated using the MRC image processing package (30, 31). Briefly, images were unbent running two cycles of CCUNBEND, and the symmetry space group was defined using ALLSPACE (32). The final map was calculated by merging images using ORIGTILTK. Projection maps were calculated using programs of the CCP4 package (33). An isotropic temperature factor (B = −500) was applied to compensate for the degradation of image amplitudes. Density contouring is at 0.25 root mean square with densities above the mean contoured by *solid lines*.

RESULTS

LH1-RC-PufX core complexes were extracted from membranes of semiaerobically grown wild type *R. sphaeroides* using an OG/sodium cholate mixture (22, 23). As previously shown, two major bands corresponding to monomeric and dimeric forms of LH1-RC-PufX complexes are found on a sucrose gradient (22, 23). Crystallization trials of both monomeric and dimeric PufX-containing core complexes led to small (~50-nm diameter) noncrystalline vesicles, whatever the rate of detergent removal (dialysis or Bio-Beads) or lipid composition (data not shown).

Since the nature of the detergent is a crucial parameter for the result of two-dimensional crystallization trials (34, 35), other detergents than the OG/cholate mixture were tried. For this purpose, the monomeric and dimeric LH1-RC-PufX bands purified in the OG/cholate sucrose gradient were dialyzed against buffers containing different detergents. After detergent exchange, the core complexes in different detergents were reconstituted, and the results were analyzed by EM. The best reconstitutions, in terms of crystallinity and size of the crystals, were obtained from PufX-containing core complexes in DOTM. The integrity of monomeric and dimeric core complexes in DOTM was confirmed by sedimentation on a sucrose gradient, absorption spectroscopy, and gel electrophoresis. As shown in Fig. 1 (*left*), sucrose gradient patterns similar to those previously described for the core complex in OG/cholate were obtained with core complexes in DOTM (23). The monomeric PufX-containing core complex (*tube 2*) ran at a density similar to that of the PufX-deleted core complex (*tube 3*), whereas the dimeric PufX-containing core complex ran at higher density (*tube 1*). The composition of core complexes in DOTM was analyzed by SDS-PAGE electrophoresis and revealed the presence of PufX (*lanes 1* and *2* in Fig. 1*A*) in contrast to the *pufX*-deleted strain (*lane 3* in Fig. 1*A*), as well as the subunits L, M, and H of RC and the subunits α/β of LH1 from wild-type *R. sphaeroides*. Finally, the spectra of core complexes in DOTM showed typical absorption peaks of pigments in native membranes at 872 and 804 nm, without detectable bands at 820 nm (disassembled LH1) or at 540–560 nm (cytochrome bc_1 complex contamination). All of these data indicate that the core complexes purified in DOTM are identical to the previously well characterized core complexes in OG/cholate (23).

For two-dimensional crystallization, monomeric or dimeric core complexes in DOTM were mixed with egg phosphatidyl-

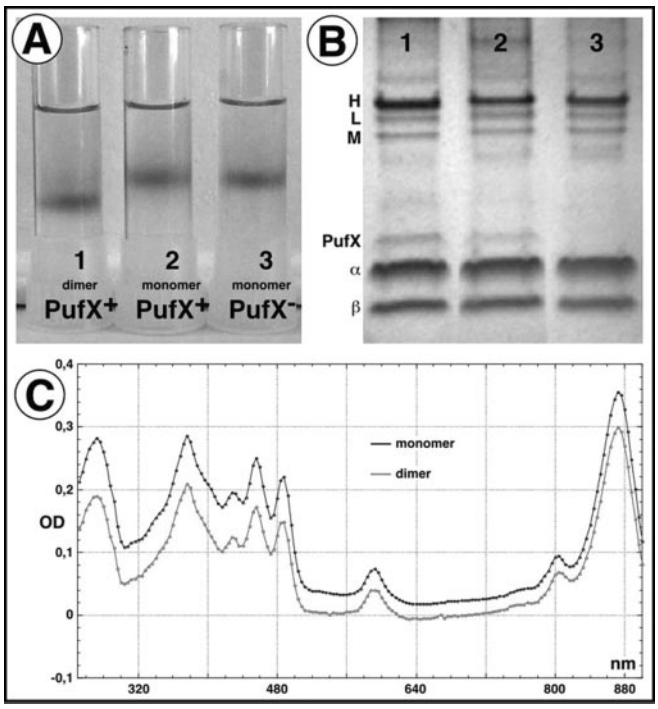

FIG. 1. **Purification of *R. sphaeroides* core complexes.** *A*, sucrose density gradients (10–35%) containing 0.1% DOTM. Purified dimeric (*tube 1*) and monomeric (*tube 2*) wild-type *R. sphaeroides* core complexes are shown. Core complex of *pufX*-deleted *R. sphaeroides* (*tube 3*) is shown. *B*, SDS-PAGE of sucrose gradient-isolated core complexes, as shown in *A*. Dimeric (*lane 1*) and monomeric (*lane 2*) wild-type *R. sphaeroides* core complexes are shown. Core complex of *pufX*-deleted *R. sphaeroides* (*lane 3*). *C*, absorption spectra of monomeric and dimeric core complexes purified in DOTM. Typical absorption bands are found: LH1 (Q_y) at 872 nm and LH1 (Q_x) at 592 nm, RC (Bchl) at 804 nm and RC (Bpheo) at 760 nm, and the carotenoid bands at 488, 456, and 432 nm.

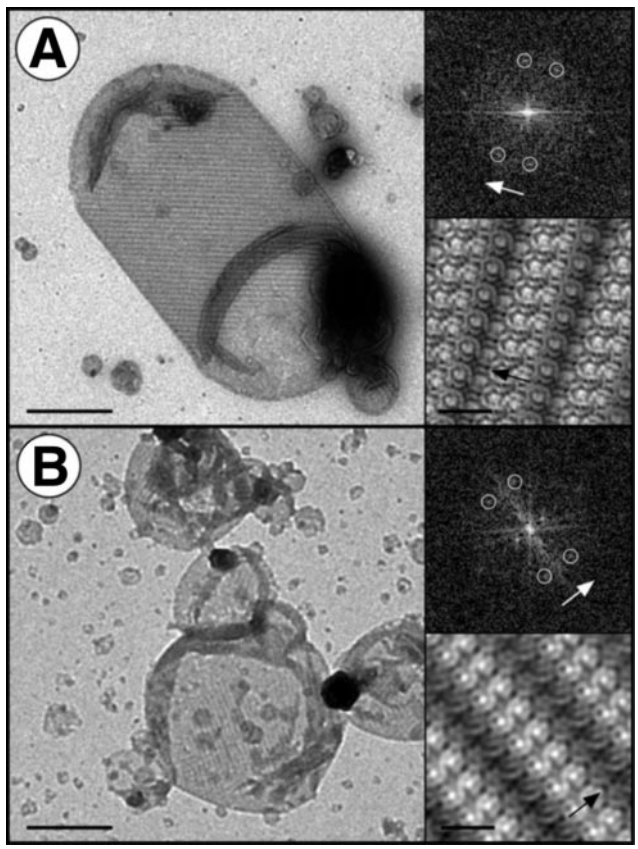

FIG. 2. **Reconstitution and two-dimensional crystallization of *R. sphaeroides* core complexes.** Low magnification electron micrographs of negatively stained samples reconstituted from purified dimeric (*A*) and monomeric (*B*) core complexes. Whereas two-dimensional crystals formed from the dimeric preparation are large (>1 μm) and coherent over large areas, crystal lattices from the monomeric preparation are only visible over smaller areas (*scale bars*; 500 nm). *Top inset*, power spectra. Spots 1,1; 1,−1; −1,1; and −1,−1 are *circled*, and the direction of the long unit cell dimension (short vector in the power spectra) is indicated by *arrows*. *Bottom inset*, filtered images (*scale bar*, 20 nm). Reconstitutions from dimeric and monomeric complexes result in identical crystal lattices of dimeric core complexes.

choline/egg phosphatidic acid (9:1, mol/mol) at lipid-to-protein ratios between 0.75 and 1.0 (w/w). Complete detergent removal at 4 °C using Bio-Beads resulted in the formation of vesicular structures whose crystallinity could be directly observed in low magnification images of negatively stained samples (Fig. 2, *A* and *B*). Strikingly, reconstitutions from both isolated monomeric and dimeric core complexes result in two-dimensional crystals constituted of dimers. Indeed, Fourier transforms (*top insets* in Fig. 2, *A* and *B*) revealed identical vector lengths for both two-dimensional crystals, and corresponding filtered images revealed the same packing arrangement of dimers in the lipid bilayer (*bottom insets* in Fig. 2, *A* and *B*). It has to be recalled that in the absence of PufX (*i.e.* with core complex from *pufX*-deleted strain), dimerization of core complexes does not occur upon reconstitution (data not shown; see also Ref. 13).

Better crystals, as judged from size (>1 × 1 μm) and packing coherence, were obtained starting from the dimeric core complex sample (Fig. 2*A*). The less coherent crystal packing obtained with the monomeric core complex was probably due to defects introduced by an incomplete dimerization of the complexes upon reconstitution.

Two-dimensional crystals formed from the dimeric preparation were embedded in vitreous ice and analyzed by cryo-EM. The two-dimensional crystals had $p22_12_1$ symmetry and unit cell dimensions of a = 381.5 Å, b = 130.0 Å, and γ = 89.5°, housing two dimeric core complexes in up-and-down orientation as clearly visible by the "S" and "Z" appearance of dimers in neighboring rows (Fig. 3, Table I). As judged from phase residual analysis, a projection map could be calculated to 26-Å resolution (Table I).

The cryo-EM projection map reveals that the core complexes assemble in a particular "S"-shaped arrangement with densities enclosed within each cavity of the "S." In agreement with general models and structural data of core complexes, the "S"-shaped densities are interpreted as LH1 assembly, and the two enclosed densities are interpreted as two RCs (1, 12, 15). However, the LH1 complex is open, forming a bow density over ~285° (see *double-headed arrow* in Fig. 3*B*) with inner and outer diameters of ~75 and ~110 Å, respectively. In the projection map of the dimer, three remarkable features can be stressed. First, there is no detectable density in the ~30-Å gap of the LH1 assembly, indicating the absence of any transmembrane segment at this position (*1* in Fig. 3*B*). Second, a maximal density is found at the dimer junction (*2* in Fig. 3*B*), whereas the rest of the projection density along the "S" is homogeneous. Third, the enclosed density originating from the RC is asymmetric, with the strongest density at the side approximately opposed to the LH1 gap (*3* in Fig. 3*B*). Since random orientation would have resulted in an averaged centered, ill defined, circular blob, the asymmetric density of the RC indicates a specific orientation of the RC within the core complex. This is in agreement with Frese *et al.* (25), who have shown such a unique orientation of the RC with respect to PufX to maximize the diffusion rate of the QH_2/Q out of and into the Q_B site.

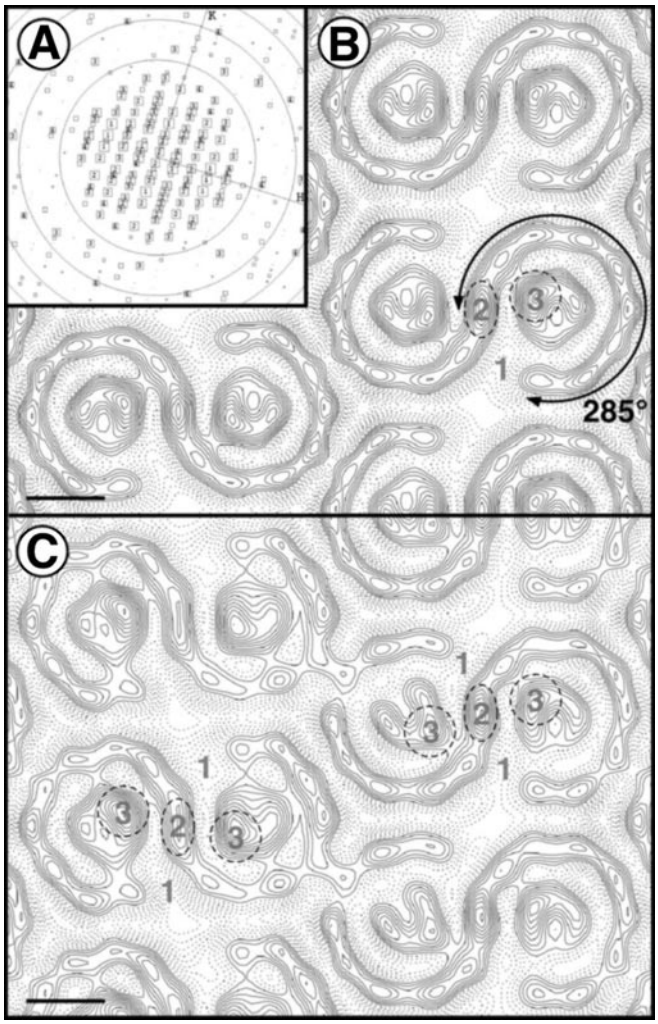

FIG. 3. **Cryo-EM analysis of the dimer core complexes from merging three two-dimensional crystal lattices.** *A*, calculated Fourier transform of a ice-embedded two-dimensional crystal. The *size* of the *boxes* indicates quality of the spot. The *circles* represent the zero passes of the contrast transfer function. *B*, symmetrized ($p22_12_1$; see Table I) projection map of the dimer core complex two-dimensional crystals at 26-Å resolution (*scale bar*, 50 Å). *C*, nonsymmetrized ($p1$) projection map of the dimer core complex two-dimensional crystals at 26-Å resolution (*scale bar*, 50 Å). In both the symmetrized and the nonsymmetrized projection maps, two lines of up-and-down oriented complexes are clearly visible. Important features are consistently found in both maps as indicated by *1*, *2*, and *3*. The LH1 assembly reveals a continuous density over ~285° (*double-headed arrow* in *B*) and a ~30-Å gap, where no density is found (*1*), the density at the dimer junction is stronger than the rest of the "S" density (10 density contour lines as compared with 3–6 density contour lines) (*2*), and the RC reveals an asymmetric density (*3*).

All of these features are consistent with the nonsymmetrized projection map, in which the unit cell contains four unique core complexes (*i.e.* two unique dimer complexes (*1*, *2*, and *3* in Fig. 3*C*).

Two-dimensional crystals and densely packed membranes were further analyzed by AFM to acquire additional topographical information on the LH1-RC-PufX assembly (Fig. 4). Two-dimensional crystals produced from the purified dimeric core complexes were adsorbed to the mica surface. Overview topographs revealed strongly corrugated ripples (Fig. 4, *A* and *B*). At higher magnification, the ripples revealed substructure corresponding to the dimeric organization of the complexes. Obviously, the incorporation of dimeric core complexes in up-and-down orientation bends the lipid membrane in opposite directions (Fig. 4*C*, *line 1*, as shown by the height profile (Fig. 4*D*, *trace 1*). Such wave shape of the membranes has hampered imaging at higher resolution by AFM and explains the strong uneven staining effect observed in negative stain electron microscopy (see *bottom insets* in Fig. 2, *A* and *B*). However, the ripples reveal a periodicity of 385 Å, consistent with the long axis of the unit cell as observed in EM (Table I) and an amplitude of 38 Å (Fig. 4*D*, *trace 1*). Along the top of the ripple axis (Fig. 4*C*, *line 2*) a periodicity of 125 Å, consistent with the short axis of the unit cell as observed in EM (Table I), and an amplitude of 8 Å are found in section analysis (Fig. 4*D*, *trace 2*).

TABLE I
Characterization of R. sphaeroides dimer core complex two-dimensional-crystals by cryo-EM

Parameter	Dimension	Error (p = 0.95)	n
Unit cell dimension (housing two dimeric complexes)	a = 381.5 Å	2.5 Å	3[a]
	b = 130.0 Å	2.5 Å	3[a]
	γ = 89.5°	1.5°	3[a]
Defocus range		4000Å–6000 Å	

	Space group	Phase residuals (*versus* other spots)	No. of spots	Phase residuals (*versus* theoretical)	No. of spots
Symmetry	$p22121$	20.8	127	11.7	108

	Resolution	n[b]	Phase residual (45° is random)
	Å		
1	57.7	19	16.3
2	40.8	14	21.8
3	33.3	11	16.8
4	28.9	11	36.9
5	25.8	12	38.7
6	23.6	11	55.0
Overall[c]	26.0	67	24.9

[a] Number of lattices in the merged image (Fig. 3).
[b] Number of unique reflections (IQ ≤ 5).
[c] Resolution cut-off was set at 26.0 Å (see also Fig. 3).

Additional information was provided by imaging membranes, in which the dimeric core complexes were reconstituted at high density but not crystalline (Fig. 4, *E* and *F*). Two different types of surfaces can be clearly identified on the membrane, corresponding to dimers inserted in up-and-down orientations in the lipid bilayer. In one orientation, the protein surfaces can be imaged and show lines of protein in dimeric arrangement (*arrow 1*), whereas in the opposite orientation, the surfaces reveal a blurry topography also arranged in lines with a similar width of about 220 Å (*arrow 2*). Such a blurry topography, covering the whole dimer surface, could be attributed to the presence of extramembranous protein domains with a high flexibility (36). This is in contrast with previous AFM topographies of different antenna complexes without PufX (15, 37, 38) and is probably related to the extramembranous domain of PufX proteins. However, the finding of dimers in a noncrystalline membrane represents additional strong evidence that dimerization is specific to PufX rather than resulting from crystallographic constraints.

DISCUSSION

A single trans-membrane protein, termed PufX in *R. sphaeroides*, has been evidenced to play a key role in the initial steps of photosynthesis. Functional studies have shown that the PufX protein is essential for photosynthetic growth and is required for a fast QH_2/Q exchange between the Q_B site in the RC and the Q_o site of the cytochrome bc_1 complex (19, 23, 25). From a structural point of view, PufX-containing core complexes have been shown to be dimeric in native membranes of *R. sphaeroides* (24). However, this finding raised strong criti-

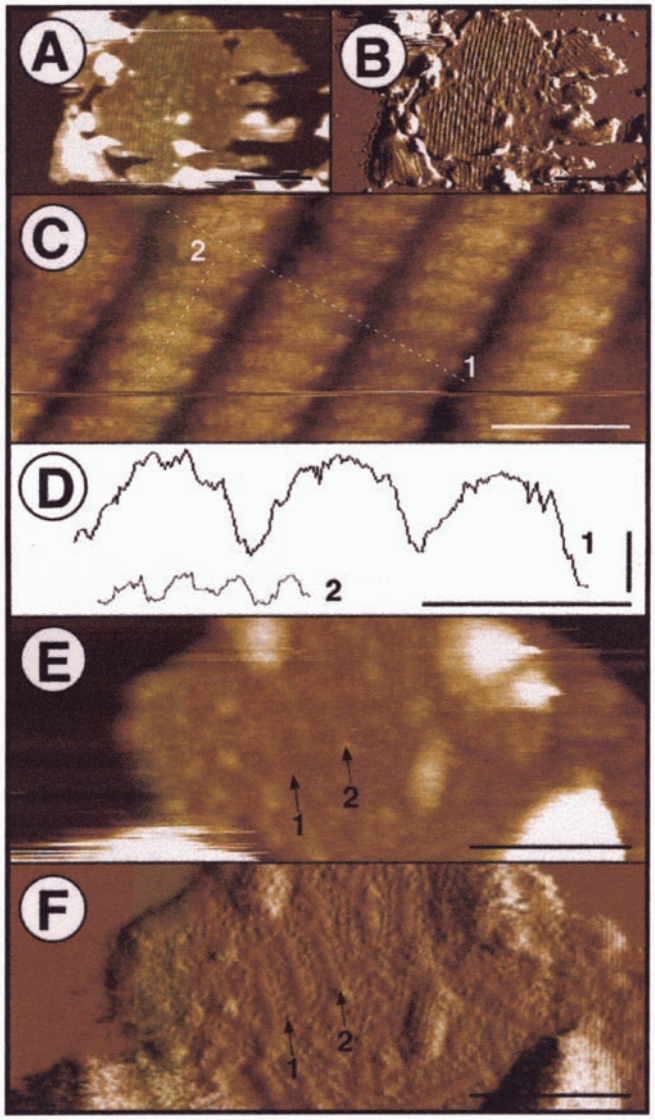

FIG. 4. **AFM analysis of the dimer core complex two-dimensional crystals and densely packed membranes.** *A*, overview topograph of a two-dimensional crystal adsorbed to the mica support. The crystal topography reveals a wavelike appearance (*scale bar*, 500 nm; *full gray scale*, 20 nm). *B*, deflection image of *topograph A*) (*scale bar*, 500 nm; *full gray scale*, 1 nm). *C*, high magnification topograph of a core complex two-dimensional crystal (*scale bar*, 50 nm; *full gray scale*, 6 nm). *D*, section analysis along the *white dashed lines* in *topograph C*). The waves appear with a periodicity of 385 Å, corresponding to the long unit cell dimension, and a corrugation of 38 Å (*line 1*). A short repetition with a periodicity of 125 Å, corresponding to the short unit cell dimension, and a corrugation of 8 Å are found perpendicular to *line 1* on top of the waves (*line 2*) (*horizontal scale bar*, 50 nm; *vertical scale bar*, 2 nm). *E*, medium magnification topograph of a noncrystalline membrane densely packed with dimer core complexes. Lines of dimeric complexes in different orientations are clearly visualized. Two different types of surfaces can be distinguished: lines of surfaces with strongly contrasted protrusions (*arrow 1*) and lines of surfaces with a blurry appearance (*arrow 2*) (*scale bar*, 200 nm; *full gray scale*, 5 nm). *F*, deflection image of *topograph E*) (*scale bar*, 200 nm; *full gray scale*, 1 nm).

cism, since the study was performed on tubular crystalline membranes gained from a LH2 deletion mutant grown under partial aerobic nonphotosynthetic conditions (16, 39, 40). Moreover, this projection map was calculated from negative stained sample, hence contrasting extramembranous domains rather than trans-membrane parts. Finally, the presence of bc_1 complex was proposed within the complex, but little structural evidence documented this hypothesis (24).

In order to obtain more insight into the role of PufX in the dimeric core complex, we have purified and two-dimensionally crystallized the dimeric PufX-containing core complexes from *R. sphaeroides*. The native core complexes of *R. sphaeroides* have been isolated by gentle solubilization with a specific mixture of OG and cholate (23), followed by a detergent exchange with DOTM, a low critical micellar concentration detergent that allowed stabilization of the dimeric core complex and improved two-dimensional crystallization. Biochemical and spectroscopic analyses (Fig. 1) were consistent with previous works on membranes or isolated complexes, indicating a dimeric core complex with a PufX/RC stoichiometry of 1:1 and a decreased number of LH1-associated Bchls per RC (23, 24, 41).

Two-dimensional crystals were analyzed by cryo-EM in order to acquire information about the protein densities of the transmembrane segments of the core complex. Despite their size and their apparent long range coherence (Fig. 2*A*), the two-dimensional crystals reconstituted from the purified dimeric core complexes provided information only to a medium resolution of 26 Å in cryo-EM (Fig. 3*A*, Table I). This unusual low resolution for an analysis by cryo-EM indicates a poor order of the two-dimensional crystals. In this context, AFM analysis of the two-dimensional crystals revealed that the up-and-down incorporation of core complexes induced a peculiar waving of the two-dimensional crystals (Fig. 4). Such bending of the membrane could be related to the tubular morphology of native membranes, in which all core complexes have the same orientation in the membrane (24, 42). It is likely that such waving hampered order at higher resolution in the two-dimensional crystals.

However, the cryo-EM map limited to 26-Å resolution revealed a dimeric assembly of the core complex with open LH1 rings. The "S"-shaped densities are interpreted as LH1 assembly, and the two central densities are interpreted as two RCs, in agreement with general models and structural data of core complexes (1, 12, 15). The inner and outer diameters of ~75 and ~110 Å, respectively, of the LH1 complex are large enough to house α/β-heterodimers with the α-polypeptide facing the ring inside (3, 4, 12) and are in agreement with the reported values of inner and outer diameters of ~70 and ~120 Å, respectively (12, 15). However, most importantly, projection density maps of the dimeric LH1-RC-PufX complexes show unequivocally gaps in the LH1 rings surrounding the RC (Fig. 3, *B* and *C*). The LH1 complexes are open, covering only slightly more than three-quarters (~285°) of a full circle, and no projection density is found within the gap (*1* in Fig. 3*B*). Since closed LH1 assemblies with similar diameters are constituted of 16 LH1 subunits (12, 15), we propose that our LH1 density contains 12 ± 1 LH1 α/β-heterodimers plus one PufX. This number of LH1 subunits is furthermore consistent with biochemical and spectroscopic measurements that have reported ~24 Bchl molecules per RC, corresponding to ~12 LH1 subunits in *R. sphaeroides* (24). In addition, the resemblance of our cryo-EM projection map with the negative stain map from the native membranes (24) indicates that no modification occurred through the purification and reconstitution procedures and that our map represents the native state of the LH1-RC-PufX assembly.

PufX is a small protein of 82 amino acids in *R. sphaeroides*. Circular dichroism, structure prediction, and proteolytic digestion have shown that PufX forms one membrane span and interacts strongly with the α-polypeptide and not with the β-polypeptide of LH1 (20, 21, 43). These data evidenced that PufX is associated in the inner α-ring of LH1 and interrupts the LH1 assembly.

In the symmetrized as well as in the nonsymmetrized projection maps, a stronger density is found (*2* in Fig. 3, *B* and *C*)

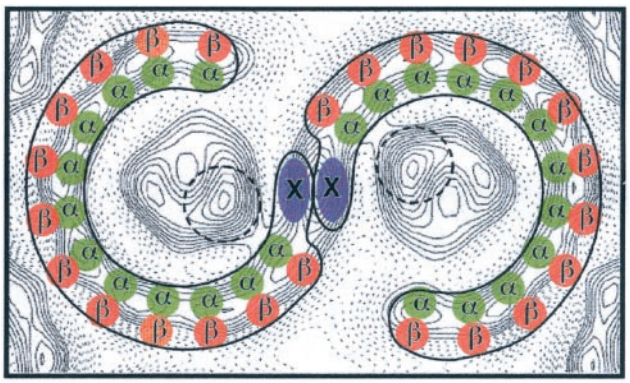

FIG. 5. **Model of the dimeric core complex.** The core complex consists of two PufX proteins, two LH1 assemblies (consisting of 12 ± 1 subunits), and two RCs. The *colored circles* corresponding to trans-membrane portions (LH1 α polypeptides in *green*, LH1 β polypeptides in *red*, and PufX proteins in *blue*) are superimposed on the projection map. The maximum densities of the RCs are *circled*, indicating a preferred orientation.

at the dimer junction. This increased density is attributed to the two PufXs, whereas identical α/β-heterodimers constitute the rest of the "S" density (Fig. 5). Indeed, a dimer of PufXs is larger (164 amino acids) than an α/β-heterodimer (104 amino acids). In particular, the C-terminal domain of PufX, of about 28 amino acids, has been predicted to form an amphipathic α-helix (44), which might increase the projection density. Reinforcing this localization, we have shown that monomeric PufX-containing core complexes dimerize upon reconstitution (Fig. 2), whereas core complexes from PufX-deleted strain never dimerize (data not shown) (13). It is likely that homologous trans-membrane interactions between two PufXs lead to dimerization of core complexes in lipid membranes. In addition, this localization solves the problem caused by the inversion of α/β-heterodimers on both sides of the "S" density (Fig. 5). Indeed, the formation of circular assembly with inner α- and outer β-rings results from homologous interaction between α/β-heterodimers. If α/β-heterodimers could assemble in both orientations, there would be no reason for the formation of circular antennas rather than random waves of LH subunits (3, 4, 9, 12, 15).

The generally proposed localization of PufX within the gap, closing the LH1 assembly, can be rejected (16, 25). Such a localization would agree with the role of PufX to interrupt the LH1 assembly but would involve the formation of two α/β-heterodimers in opposite orientation at the dimer junction. In addition, these α/β-heterodimers at the dimer junction should also have the property to induce dimerization, since the two PufXs would be separated from each other, excluding their direct role in dimer formation. Furthermore, the presence of a highly tilted trans-membrane helix in the gap that would produce weak densities in the projection map is also unlikely, since to fill a gap of ~30-Å length in a lipid membrane of ~40-Å thickness, a trans-membrane helix of ~50-Å length would be required. Such a long helix is in disagreement with hydropathy analysis of PufX (21) and with data reporting a minimal core portion of 25 amino acids of PufX to be sufficient to inhibit the LH1 assembly (21, 22). Finally, a possible localization of PufX at the peripheral ends of the "S" can be rejected for the same reasons.

However, if PufX is located at the dimer junction and not within the gap, why are there no additional LH1 subunits that close the three-quarter circle, and what is the role of the gap? A first proposal would be to interpret the gap as a channel for the QH_2/Q exchange between the RC and the bc_1 complex. However, in addition to the fact that a 30-Å-wide gap is excessively large for a QH_2/Q channel, it would still be unclear how the assembly of the core complex could know when to stop the assembly of additional LH1 around RC (42). A second proposal would be to consider the gap as a docking site for the bc_1 complex and more specifically for its subunit IV. In this context, several results have suggested that this subunit (14 kDa), found so far only in the isolated bc_1 from *R. sphaeroides*, was essential for photosynthetic electron transfer activity (24). Indeed, it has been shown that subunit IV is absent in aerobically grown *R. sphaeroides*, although the bc_1 complex is fully functional for respiration (45). Interestingly, a study of the time-dependent assembly of the photosynthetic unit has shown that subunit IV of bc_1 is, together with PufX and the H subunit of the RC, the first protein to be present, followed by the synthesis of LH1 α/β polypeptides, leading to the encircling of the RC (43). Thus, it could be proposed that, at an early stage of assembly, subunit IV is used as a placeholder to hamper further LH1 subunit addition at the position where we have now observed a gap in the purified LH1-RC-PufX complexes.

In conclusion, we have been able, based on reconstitution experiments and cryo-EM analysis of two-dimensional crystals, to gain much evidence for a localization of PufX at the dimer junction and for its role as a structural organizer within the core complex of *R. sphaeroides*. We suggest that PufX could act as a symmetry breaker to prevent the clustering of RC-LH1 complexes into large hexagonal arrangements, as observed for several species of purple bacteria without *pufX* (6, 8, 15, 46). Due to this suggestion, PufX-induced core dimerization would facilitate indirectly the functional interplay of RC-LH1 core complexes with other components of the photosynthetic unit like LH2 and bc_1 complex. Such a hypothesis will be tested by future AFM analysis of native membranes, consisting of all components of the photosynthetic chain, LH2, LH1, PufX, RC, and bc_1 complexes.

Acknowledgments—We thank Dr. Olivier Lambert for images taken with the 200FEG electron microscope, M. Dezi for help in the biochemical analysis, and G. Venturoli for fruitful discussions.

REFERENCES

1. Hu, X., Ritz, T., Damjanovic, A., Autenrieth, F., and Schulten, K. (2002) *Q. Rev. Biophys.* **35,** 1–62
2. Deisenhofer, J., Epp, O., Miki, K., Huber, R., and Michel, H. (1985) *Nature* **318,** 618–624
3. McDermott, G., Prince, S. M., Freer, A. A., Hawthornthwaite-Lawless, A. M., Papiz, M. Z., Cogdell, R. J., and Isaacs, N. W. (1995) *Nature* **374,** 517–521
4. Koepke, J., Hu, X., Muenke, C., Schulten, K., and Michel, H. (1996) *Structure* **4,** 581–597
5. Xia, D., Yu, C. A., Kim, H., Xia, J. Z., Kachurin, A. M., Zhang, L., Yu, L., and Deisenhofer, J. (1997) *Science* **277,** 60–66
6. Miller, K. R. (1982) *Nature* **300,** 53–55
7. Stark, W., Kühlbrandt, W., Wildhaber, I., Wehrli, E., and Muhlethaler, K. (1984) *EMBO J.* **3,** 777–783
8. Engelhardt, H., Engel, A., and Baumeister, W. (1986) *Proc. Natl. Acad. Sci. U. S. A.* **83,** 8972–8976
9. Karrasch, S., Bullough, P. A., and Ghosh, R. (1995) *EMBO J.* **14,** 631–638
10. Walz, T., and Ghosh, R. (1997) *J. Mol. Biol.* **265,** 107–111
11. Stahlberg, H., Dubochet, J., Vogel, H., and Ghosh, R. (1998) *J. Mol. Biol.* **282,** 819–831
12. Jamieson, S. J., Wang, P., Qian, P., Kirkland, J. Y., Conroy, M. J., Hunter, C. N., and Bullough, P. A. (2002) *EMBO J.* **21,** 3927–3935
13. Walz, T., Jamieson, S. J., Bowers, C. M., Bullough, P. A., and Hunter, C. N. (1998) *J. Mol. Biol.* **282,** 833–845
14. Ikeda-Yamasaki, I., Odahara, T., Mitsuoka, K., Fujiyoshi, Y., and Murata, K. (1998) *FEBS Lett.* **425,** 505–508
15. Scheuring, S., Seguin, J., Marco, S., Lévy, D., Robert, B., and Rigaud, J. L. (2003) *Proc. Natl. Acad. Sci. U. S. A.* **100,** 1690–1693
16. Loach, P. A. (2000) *Proc. Natl. Acad. Sci. U. S. A.* **97,** 5016–5018
17. Farchaus, J. W., Barz, W., Grünberg, H., and Oesterhelt, D. (1992) *EMBO J.* **11,** 2779–2788
18. Lilburn, T. G., Haith, C. E., Prince, R. C., and Beatty, J. T. (1992) *Biochim. Biophys. Acta* **1100,** 160–170
19. Barz, W., Vermeglio, A., Francia, F., Venturoli, G., Melandri, B., and Oesterhelt, D. (1995) *Biochemistry* **34,** 15248–15258
20. Recchia, P. A., Davis, C. M., Lilburn, T. G., Beatty, J. T., Parkes-Loach, P. S., Hunter, C. N., and Loach, P. A. (1998) *Biochemistry* **37,** 11055–11063
21. Parkes-Loach, P. S., Law, C. J., Recchia, P. A., Kehoe, J., Nehrlich, S., Chen, J., and Loach, P. A. (2001) *Biochemistry* **40,** 5593–5601
22. Francia, F., Wang, J., Venturoli, G., and Oesterhelt, D. (2002) *Eur. J. Biochem.*

269, 1877–1885
23. Francia, F., Wang, J., Venturoli, G., Melandri, B., Barz, W., and Oesterhelt, D. (1999) *Biochemistry* **38,** 3834–3845
24. Jungas, C., Ranck, J.-L., Rigaud, J.-L., Joliot, P., and Vermeglio, A. (1999) *EMBO J.* **18,** 534–542
25. Frese, R. N., Olsen, J. D., Branvall, R., Westerhuis, W. H., Hunter, C. N., and van Grondelle, R. (2000) *Proc. Natl. Acad. Sci. U. S. A.* **97,** 5197–5202
26. Lévy, D., Mosser, G., Lambert, O., Moeck, G. S., Bald, D., and Rigaud, J. L. (1999) *J. Struct. Biol.* **127,** 44–52
27. Schägger, H., and von Jagow, G. (1987) *Anal. Biochem.* **166,** 368–379
28. Rigaud, J., Lévy, D., Mosser, G., and Lambert, O. (1998) *Eur. Biophys. J.* **27,** 305–319
29. Schabert, F. A., and Engel, A. (1994) *Biophys. J.* **67,** 2394–2403
30. Henderson, R., Baldwin, J. M., Ceska, T. A., Zemlin, F., Beckman, E., and Downing, K. H. (1990) *J. Mol. Biol.* **213,** 899–929
31. Crowther, R. A., Henderson, R., and Smith, J. M. (1996) *J. Struct. Biol.* **116,** 9–16
32. Valpuesta, J. M., Carrascosa, J. L., and Henderson, R. (1994) *J. Mol. Biol.* **240,** 281–287
33. Collaborative Computational Project Number 4 (1994) *Acta Crystallogr.* **4,** 760–763
34. Rigaud, J., Chami, M., Lambert, O., Lévy, D., and Ranck, J. (2000) *Biochim. Biophys. Acta* **23,** 112–128
35. Chami, M., Pehau-Arnaudet, G., Lambert, O., Ranck, J., Lévy, D., and Rigaud, J. (2001) *J. Struct. Biol.* **133,** 64–74
36. Scheuring, S., Ringler, P., Borgina, M., Stahlberg, H., Müller, D. J., Agre, P., and Engel, A. (1999) *EMBO J.* **18,** 4981–4987
37. Scheuring, S., Reiss-Husson, F., Engel, A., Rigaud, J.-L., and Ranck, J.-L. (2001) *EMBO J.* **20,** 3029–3035
38. Scheuring, S., Seguin, J., Marco, S., Lévy, D., Breyton, C., Robert, B., and Rigaud, J.-L. (2003) *J. Mol. Biol.* **325,** 569–580
39. Vermeglio, A., and Joliot, P. (1999) *Trends Microbiol.* **7,** 435–440
40. Crofts, A. R. (2000) *Trends Microbiol.* **8,** 107–108
41. McGlynn, P., Hunter, C. N., and Jones, M. R. (1994) *FEBS Lett.* **349,** 349–353
42. Westerhuis, W. H., Sturgis, J. N., Ratcliffe, E. C., Hunter, C. N., and Niederman, R. A. (2002) *Biochemistry* **41,** 8698–8707
43. Pugh, R. G., McGlynn, P., Jones, M. R., and Hunter, C. N. (1998) *Biochim. Biophys. Acta* **1366,** 301–316
44. Rost, B., Sander, C., and Schneider, R. (1994) *Comput. Appl. Biosci.* **10,** 53–60
45. Chen, Y. R., Usui, S., Yu, C. A., and Yu, L. (1994) *Biochemistry* **33,** 495–500
46. Meckenstock, R. U., Krusche, K., Staehelin, L. A., Cyrklaff, M., and Zuber, H. (1994) *Biol. Chem. Hoppe Seyler.* **375,** 429–438

Structural Role of PufX in the Dimerization of the Photosynthetic Core Complex of *Rhodobacter sphaeroides*

Simon Scheuring, Francesco Francia, Johan Busselez, Bruno Andrea Melandri, Jean-Louis Rigaud and Daniel Lévy

J. Biol. Chem. 2004, 279:3620-3626.
doi: 10.1074/jbc.M310050200 originally published online October 27, 2003
